Kinetic insights into agonist-dependent signalling bias at the pro-inflammatory G-protein coupled receptor GPR84

Vincent B. Luscombe [a], Luis Alberto Baena-López [a], Carole J.R. Bataille [b], Angela J. Russell [b,c], David R. Greaves [a,*]

[a] *Sir William Dunn School of Pathology, South Parks Rd, University of Oxford, Oxford, Oxfordshire, OX1 3RE, United Kingdom*
[b] *Department of Chemistry, Mansfield Rd, University of Oxford, Oxford, Oxfordshire, OX1 3TA, United Kingdom*
[c] *Department of Pharmacology, Mansfield Rd, University of Oxford, Oxford, Oxfordshire, OX1 3TA, United Kingdom*

ARTICLE INFO

ABSTRACT

GPR84 is an orphan G-protein coupled receptor (GPCR) linked to inflammation. Strategies targeting GPR84 to prevent excessive inflammation in disease are hampered by a lack of understanding of its precise functional role. We have developed heterologous cell lines with low GPR84 expression levels that phenocopy the response of primary cells in a label-free cell electrical impedance (CEI) sensing system that measures cell morphology and adhesion. We then investigated the signalling profile and membrane localisation of GPR84 upon treatment with 6-OAU and DL-175, two agonists known to differentially influence immune cell function. When compared to 6-OAU, DL-175 was found to exhibit a delayed impedance response, a delayed and suppressed activation of Akt, which together correlated with an impaired ability to internalise GPR84 from the plasma membrane. The signalling differences were transient and occurred only at early time points in the low expressing cell lines, highlighting the importance of receptor number and kinetic readouts when evaluating signalling bias. Our findings open new ways to understand GPR84 signalling and evaluate the effect of newly developed agonists.

1. Introduction

GPR84 is an orphan GPCR that is transcriptionally upregulated by inflammatory mediators and acts as an enhancer of immune cell function. For example, the pathogen-associated molecular patterns derived from lipopolysaccharides cause 10 to 100-fold increases in *Gpr84* expression in primary human and murine macrophages and macrophage cell lines as well as primary human and murine neutrophils, whereas IL-4 reduces *Gpr84* expression in primary human and murine macrophages (Puengel et al., 2020; Recio et al., 2018). Activation of GPR84 leads to an induction of cell-type specific inflammatory processes, including cytokine secretion, chemotaxis, phagocytosis, bacterial adhesion, reactive oxygen species production, degranulation, and NETosis (Gaidarov et al., 2018; Peters et al., 2022; Recio et al., 2018; Sundqvist et al., 2018; Suzuki et al., 2013). Although the function of GPR84 *in vivo* is not fully understood, its activity has been linked to various diseases such as

obesity, non-alcoholic fatty liver disease, and ulcerative colitis, through mechanisms that remain elusive. Early reports indicated that GPR84 could respond to medium-chain fatty acids (MCFAs), thus suggesting it could act as a sensor for dietary fatty acids such as capric acid. However, inconsistencies in the potency and expression of this receptor-ligand pairing (Luscombe et al., 2020), as well as the recent clinical failures of GPR84 antagonists in ulcerative colitis and idiopathic pulmonary fibrosis (Cottin et al., 2021; Khalil et al., 2019; Labéguère et al., 2020), highlight that the therapeutic efficacy of blocking GPR84 signalling is still unknown. This lack of understanding is evident at both the disease level and at the molecular level, with the principal questions being: what is the endogenous GPR84 agonist that is being blocked and what downstream pathways are important to turn off in order to achieve anti-inflammatory effects *in vivo*?

Improving our molecular understanding of GPR84 signalling and the effector pathways required for its function in immune cells could aid in

---

the optimisation of drug candidates to block or promote relevant pathways. For example, it might be desirable to inhibit the pathological recruitment of immune cells and activation of the cytokine storm at a site of injury while maintaining, or even promoting phagocytosis. Previous studies have identified the GPR84 selective agonists 6-OAU and DL-175. While 6-OAU is a balanced agonist able to activate the G_i as well as β-arrestin pathways, DL-175 is a G-protein biased agonist that is unable to recruit β-arrestins (Lucy et al., 2019). When comparing 6-OAU and DL-175 in a human-derived U937 macrophage-like cell line it is apparent that 6-OAU induces both chemotaxis and phagocytosis, while DL-175 maintains phagocytosis without any chemotactic effect (Lucy et al., 2019). These experiments suggest that GPR84 activation can be as pharmacologically tuneable as other immune cell receptors such as those for host defence (e.g. complement component and formyl peptide receptors), danger signalling (e.g. chemokine and purinergic receptors), and quorum sensing (e.g. aryl hydrocarbon and bitter taste receptors) (Dahlgren et al., 2016; Gaida et al., 2016; Greaves and Schall, 2000; McDonald et al., 2010; Moura-Alves et al., 2019). Our aim in this study was to characterise the molecular basis for this differential activation of GPR84.

In this manuscript we investigate GPR84 signalling using two agonists known to differentially influence immune cell function, 6-OAU and DL-175. We have quantified their effect on cell morphology, downstream kinase phosphorylation, and receptor internalisation. Our results reveal differences in effector protein activation and receptor dynamics over time, consistent with the biased signalling of DL-175.

2. Materials and methods

2.1. Development of CHO-HA-GPR84 monoclones

Gene fragments containing *Homo sapiens* (NCBI Reference Sequence: NM_020370.3) and *Mus musculus* (NCBI Reference Sequence: NM_030720.3, codon optimised) (O'Leary et al., 2016) GPR84 coding sequences preceded by an N-terminal HA-tag in a Kozak setting and flanked by restriction enzyme sites for AflII and XbaI were designed using SnapGene® software (from Insightful Science; available at snapgene.com) and synthesised by Twist Biosciences (San Francisco, CA). Fragments were PCR amplified, electrophoresed, gel extracted, and then sequence verified by Source BioScience (Nottingham, UK). HA-GPR84 fragments were cloned into a pcDNA3.1+ mammalian expression vector by sticky end restriction enzyme cloning. *E. coli* DH5α cells were transformed and colonies possessing recombinant plasmids were screened for by restriction enzyme digests, followed by plasmid scale up and DNA sequence verification.

CHO–K1 cells were transfected with HA-GPR84-pcDNA3.1+ using the Amaxa® Nucleofector™ 2b device (Lonza AAB-1001) and Cell Line Nucleofector® Kit T (Lonza VVCA-1002, as per the manufacturer's protocol) before selection pressure was applied using G418 (600 μg/mL; Thermo 10131027) for 10–14 days. Polyclonal cells were sorted by limiting dilution into 96-well plates and left to grow for 10–14 days. During outgrowth, clones were tested for responses to 6-OAU (10 μM) in a single point cAMP assay. Hits were later confirmed by response to three concentrations of 6-OAU, followed by side-by-side concentration-response curves and Western blots after 4 weeks of culture. Monoclonal CHO cell lines were selected based on their functional response to 6-OAU, positive α-HA-GPR84 antibody reactivity, and longevity in culture.

2.2. Cell culture

All CHO Cell lines and were maintained and plated overnight in Ham's F12 (Thermo 21765029) supplemented with 10% fetal bovine serum (FBS; Sigma F4135), 19 mM HEPES (Sigma H0887), and 1% penicillin-streptomycin (Gibco 15140122). When propagating GPR84 cell lines 600 μg/mL G418 was included.

Murine Bone Marrow Derived Macrophages (mBMDMs) were harvested and grown as described previously (Recio et al., 2018), then stored frozen in FBS + 10% DMSO (Sigma D8418). mBMDMs were thawed and plated with the inclusion of 100 ng/mL lipopolysaccharide (Merck L4391) to up-regulate GPR84 expression (Recio et al., 2018).

2.3. Assay for cAMP production

Cells were plated at 15,000 cells / 20 μL / well in a white 384-well microplate (Greiner 781098) 24 h before stimulation with forskolin (25 μM) and agonist for 30 min at 37 °C, or pre-incubated for 24 h with pertussis toxin (100 ng/mL) or 30 min with antagonist 8 (30 μM) at 37 °C, then stimulated with forskolin (50 μM) and agonist for 30 min at 37 °C. Drugs were dissolved in DMSO and prepared in PBS + 0.1% BSA. Cell lysis and detection of cAMP was performed using the HitHunter® cAMP Assay for Small Molecules (DiscoverX 90-0075SM2 as per the manufacturer's instructions). Luminescence was measured 18–24 h after the final step on a PHERAstar® *FS* microplate reader (BMG Labtech).

2.4. Western blotting and assay for ERK and Akt phosphorylation

Cells were seeded at 300,000 (GPR84 expression) or 500,000 (ERK and Akt assay) cells / 2 mL / well in a 6-well plate 48 h prior to harvesting. Cells were placed on ice to terminate the assay and gently washed twice with 3 mL of ice-cold PBS, before lysis with 50 μL 1.5X RIPA buffer with protease and phosphatase inhibitors. Lysates were rapidly scraped and frozen at −80 °C. Clarified protein concentrations were determined by Pierce™ BCA Protein Assay (Thermo 23225) before 25 μg / lane was resolved by SDS-PAGE under reducing conditions in 10% NuPAGE Bis-Tris gels (Thermo NP0302BOX). Proteins were transferred to a nitrocellulose membrane (Thermo LC2000), blocked with 5% non-fat dry milk in TBS for 1 h at room temperature, then probed overnight at 4 °C with primary antibodies in TBST + 5% non-fat dry milk (Mouse α-p-Akt CST 4051, Rabbit α-Akt CST 9272, Rabbit α-p-ERK CST 9101, and Mouse α-ERK CST 9107 for Akt/ERK, or Rabbit α-HA CST 3724 with Mouse α-ERK CST 9107, or Rat α-HA Merck 11867423001 with rabbit anti-β-actin CST 4967 for receptor expression). Secondary antibody in TBST + 5% non-fat dry milk (Goat α-Mouse DL680 Thermo 35519 and Goat α-Rabbit DL800 Thermo SA5-10036; or Goat α-Rat DL800 Thermo SA5-10024, and Goat α-Rabbit DL680 Thermo 35569) was applied for 1 h at room temperature before the membrane was dried and visualised on an Odyssey Sa Infrared Imaging System (LI-COR Biosciences) on the 700 nm and 800 nm channels simultaneously. Band signal intensity was quantified in ImageStudio Lite v5.2 (LI-COR Biosciences).

When assaying for ERK and Akt phosphorylation cells were serum starved for 18–24 h and pre-incubated with vehicle (2 h), or Akt inhibitor MK-2206 (10 μM, 24 h) and MEK inhibitor U0126 (10 μM, 2 h) as negative controls prior to stimulation with agonist. Agonists 6-OAU (1 μM) and DL-175 (1 μM) were dissolved at 12X in serum-free media + 0.1% BSA and warmed to 37 °C before addition at the appropriate time. Calyculin A (60 nM, 30 min) and FBS (10%, 10 min) were used as positive controls for ERK and Akt phosphorylation.

2.5. Cell electrical impedance assay

The xCELLigence Real-Time Cell Analysis (RTCA) SP instrument (Agilent) was used to measure cell electrical impedances (Solly et al., 2004) as per the manufacturer's protocol. Numerous cellular processes can be captured with changes in impedance measurements, including macrophage adherence and spreading, cell morphology changes due to cytoskeletal rearrangements, cell migration, and cell cytotoxicity responses (Solly et al., 2004). Background impedance measurements were taken in each well of an RTCA E-Plate 96 PET (Agilent 300600910) using 50 μL of pre-warmed media. Cells were trypsinised and suspensions added at 40,000 cells / 100 μL / well for CHO cell lines, or 50,000 for

mBMDMs, equilibrated at room temperature for 30 min, then incubated for 20–22 h in media supplemented with 10% FBS. Drugs were dissolved in DMSO and prepared at 27X in serum-free media + 0.1% BSA before addition to the E-Plate. Antagonist 8 or vehicle (DMSO) was added 2 h prior to stimulation with agonist. Pertussis toxin (dissolved in dH$_2$O) was pre-incubated for 24 h, and these conditions were controlled for with vehicle additions 2 h prior to stimulation. Impedance measurements were taken every 30 s for 1 h following inhibitor and agonist additions.

Cell Index (CI) measurements were exported and normalised to the time point immediately prior to drug addition. As all conditions were tested in duplicate, these were first averaged, then normalised to the vehicle-vehicle (baseline) condition, yielding baseline normalised cell index values (BNCI).

2.6. Receptor internalisation assay

Cells were plated at 12,000 cells / 20 µL / well in a black glass bottom 384-well microplate (Greiner 781892) coated with collagen I and incubated overnight. Drugs were dissolved at 5X in assay media and added to be incubated for 5–60 min at 37 °C / 5% CO$_2$. The plates were placed on ice for 2 min to halt further internalisation and washed with PBS x 4 using an AquaMax 2000 microplate washer (Molecular Devices). Cells were then fixed in 4% methanol-free formaldehyde for 20 min, washed with PBS x 4, and blocked for 45 min in PBS + 1% BSA. Without permeabilising cell membranes, thereby preventing intracellular epitope recognition by antibodies (Finlay et al., 2016), the cells were washed with PBS x 4, then incubated with Rat α-HA 1° antibody (Merck 11867423001) for 2 h at room temperature. Cells were then washed in PBS x 8 and incubated with Donkey α-Rat AF488 2° antibody (Thermo A-21208) and Hoechst 33342 for 1 h at room temperature. Cells were then washed with PBS x 8 and stored at 4 °C overnight. Experiments comparing surface expression between cell lines included Phalloidin AF555 (Thermo A34055) during the primary incubation step.

Images were captured using the EVOS M7000 (Invitrogen) using a 20X 0.75 NA objective lens. Each condition was assayed in triplicate, and in each replicate well 3 non-contiguous images were taken (Fig. S1A). An imageJ macro was then used to merge channels from each field of view into a single image stack. Image segmentation was performed on these multichannel images using the ZeroCostDL4Mic Cellpose 2D v1.15 notebook, a generalist method employing deep-learning to segment cell bodies and generate masks for each cell (Stringer et al., 2021; von Chamier et al., 2021). Default parameters were used with the cytoplasm2 model (Object_diameter=0, Flow_threshold=0.4, mask_threshold=0). A second ImageJ macro then used the ImageJ plugin ijp-LaRoMe from BioImaging And Optics Platform (https://github.com/BIOP) (Waisman et al., 2021) to convert labels created by Cellpose to regions of interest (ROIs) using the "Label image to ROIs" command and then batch process measurements within each ROI in each channel (Fig. S1B). This allowed for the rapid analysis of ~1,000 ROIs in each well. The mean GFP fluorescence intensity of each of the ~1,000 ROIs was first averaged, producing a single value per well. These values, correlating to the average surface receptor on cells, were averaged between technical replicates and then normalised to time-matched vehicle (DMSO) conditions.

One-phase decay slopes were fitted to the time-course data, which were also re-plotted as concentration-response curves using a three-parameter curve fitting model in GraphPad Prism (v9.4.1). Internalisation descriptors from the curve fits were conducted on each replicate before being pooled between biological replicates. Normalised values of nett surface receptor from independent biological replicates were pooled and presented in Prism.

2.7. Chemicals and chemical synthesis

Purchased from commercial vendors: 6-OAU (Cayman Chemical

17687), DL-175 (Tocris 7082), capric acid (Sigma C1875), myristic acid (Sigma M2138), forskolin (Cambridge Bioscience SM18-2), cmpd101 (Tocris 5642), MK-2206 (APExBio A3010), U0126 (Cell Guidance Systems SM106), calyculin A (ab141784), pertussis toxin (Tocris 3097), DMSO (Sigma D8418), Tween-80 (Sigma 8.22187), BSA (Sigma A7906), PBS (Thermo 14190094), Tris-buffered saline (Sigma T5941, T6066, S9888), Tween-20 (Sigma P1379), RIPA buffer (Millipore 20-188), protease and phosphatase inhibitors (Sigma 11836170001, P5726, P5726; CST 8553), non-fat dry skim milk powder (Sigma 70166), collagen I (Merck C3867), formaldehyde (Thermo 28906), Hoechst 33342 (ImmunoChemistry technologies 639).

Antagonist 8 (2-((1,4-Dioxan-2-yl)methoxy)-9-hydroxy-6,7-dihydro-4H-pyrimido[6,1-a]isoquinolin-4- one, CAS ID 1445846-30-9) was synthesised as previously described [2]. DL-222 (2-(2-((4-chloronaphthalen-1-yl)oxy)ethyl)pyridine 1-oxide) was synthesised as previously described [11].

Synthesis of (*rac*)-3-hydroxy capric acid is provided in Supplementary Information.

3. Results

3.1. Development and characterisation of CHO-HA-GPR84 cell lines

We have previously described the effects of 6-OAU and DL-175 on commercially available human GPR84 CHO cell lines, primary human monocytes and mBMDMs, and the human U937 cell-line (Lucy et al., 2019). To determine the functional similarities between the mouse and human receptor, we generated several transgenic GPR84 CHO cell lines. Due to a lack of GPR84-specific antibodies (Recio et al., 2018) (Fig. S2) an N-terminal HA-tag was included to facilitate antibody recognition (Fig. S3). We isolated three clones expressing different levels of GPR84. One of these clones expressed high levels of the human protein, while two separate clones expressed low levels of the human and mouse orthologues of GPR84 respectively (Fig. 1A and B). Protein resolution by SDS-PAGE and probing for the HA-tag showed a diffuse GPR84 band strongly expressed by the CHO-HA-hGPR84 #7F12 clone, with more weak expression in the CHO-HA-hGPR84 #3E11 and CHO-HA-mGPR84 #18E7 clones, and no detection in the commercial CHO-hGPR84 (DiscoverX) and CHO–K1 parental cell lines, both of which lack the HA-tag epitope (Fig. 1A). The high expressing clone was then probed with an alternative α-HA primary antibody which demonstrated expression of GPR84 with two distinct bands between 55 and 70 kDa, as well as a higher apparent molecular weight band near 120 kDa (Fig. 1B). A similar pattern was observed by Marsango et al. (2022b) expressing the human form of GPR84 tagged with eYFP in HEK293 cells. The smaller bands were suggested to represent different post-translationally modified versions of the receptor, while the high molecular weight band may be aggregated or dimeric forms. The high expressing CHO-HA-hGPR84 #7F12 clone was also demonstrated to have higher surface receptor expression of the HA-tag than the low expressing clones, which were found to be indistinguishable from the no-epitope and CHO–K1 controls (Fig. 1C–G, Fig. S4).

As expected, receptor expression levels were found to correlate with agonist potency. When tested in a functional assay for inhibition of forskolin-stimulated cAMP production, the high expressing cell line #7F12 responded with the highest agonist potency (Fig. 1H), followed by the commercial CHO-hGPR84 DiscoverX cell line (Fig. 1I), then the low expressing human #3E11 (Fig. 1J) and mouse #18E7 (Fig. 1K) cell lines. In all three human GPR84 cell lines 6-OAU was equally potent as DL-175, yet in the mouse GPR84 cell line 6-OAU was 6x less potent than DL-175 (Table 1, unpaired *t*-test p = 0.01). We also observed a loss of effect with 6-OAU at the top two concentrations in the low expressing cell lines (Fig. 1J, K), i.e. U-shaped concentration-response curves, but all cell lines had full efficacy responses at or below 1 µM and shared low nanomolar EC$_{50}$'s. The response to 1 µM agonist was absent in CHO–K1 parental cells (Fig. 1L), and could be blocked by pre-treatment with
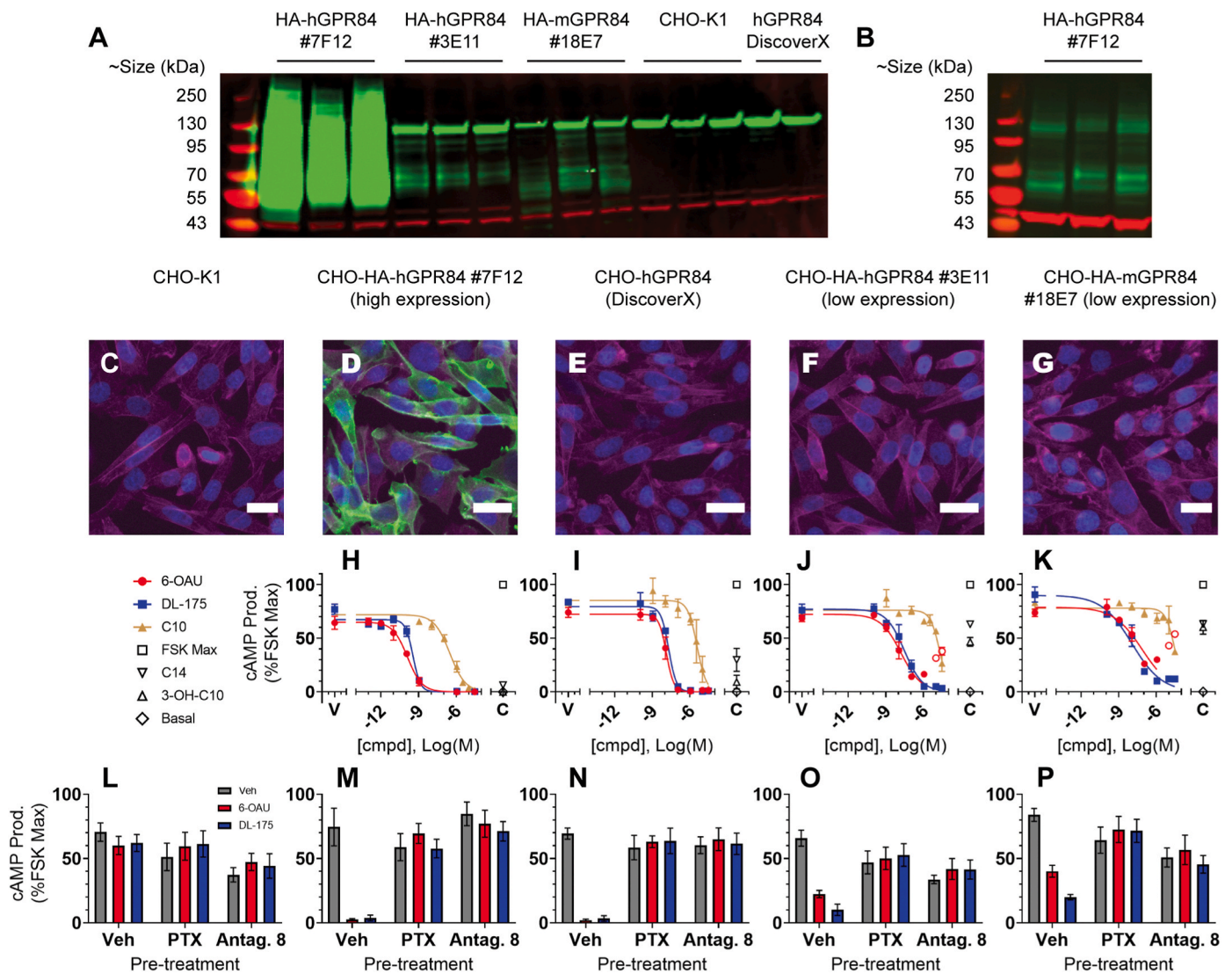
Fig. 1. Characterisation of human and mouse GPR84 cell lines by receptor. Total GPR84 expression in each cell line following protein resolution by SDS-PAGE and Western blotting against the HA-tag (green) using rabbit α-HA primary antibody and ERK1/2 (red) (A), or rat α-HA primary antibody and β-actin (red) (B). Three independent protein lysates from each cell line were developed on a single gel. The hGPR84 DiscoverX cell line expresses GPR84 but not the HA-tag epitope. (C–G) Surface GPR84 expression in each cell line following immunolabelling of the HA-tag (green), F-actin (magenta), and nuclei (blue) without cell membrane permeabilisation. Images acquired using a 20X 0.75 NA objective lens, scale bar = 25 μm. (H–K) Concentration-response curves of cAMP production by cell line following 30 min stimulation with agonist. Points represent mean ± SEM, n = 3–4, each experiment performed in triplicate. (L–P) Responses to 1 μM agonist following pre-treatment with pertussis toxin (100 ng/mL) or antagonist 8 (30 μM). Bars represent mean ± SEM, n = 3, each experiment performed in triplicate. C10, capric acid; 3-OH-C10, 3-hydroxy capric acid; C14, myristic acid; PTX, pertussis toxin.

Table 1
cAMP Potency of GPR84 agonists in human and mouse GPR84 cell lines.

Compound	GPR84 cAMP Potency EC$_{50}$ (nM) [pEC50 ± SEM]			
	Human #7F12 (high expression)	Human (DiscoverX)	Human #3E11 (low expression)	Mouse #18E7 (low expression)
6-OAU	0.120 [9.92 ± 0.15]	1.16 [8.94 ± 0.31]	15.3 [7.81 ± 0.25]	66.0 [7.18 ± 0.21]
DL-175	0.356 [9.45 ± 0.10]	1.98 [8.70 ± 0.16]	29.0 [7.54 ± 0.20]	11.0 [7.96 ± 0.21]
Capric acid	305 [6.52 ± 0.18]	3,595 [5.44 ± 0.39]	>10,000 [<5.00]	>10,000 [<5.00]

pertussis toxin or antagonist 8 in all GPR84 expressing cell lines (Fig. 1M-P). Similar potency shifts were seen when comparing capric acid, which achieved nanomolar EC$_{50}$'s in the high expressing cell line but high micromolar EC$_{50}$'s in the low expressing cell lines (Table 1).

Furthermore, neither 3-hydroxy capric acid, capric acid, or myristic acid caused full efficacy cAMP responses in low expressing cell lines (Fig. 1J and K).

3.2. 6-OAU and DL-175 elicit distinct impedance phenotypes in mBMDMs and heterologous CHO expression systems

We have previously demonstrated the usefulness of impedance sensing as a label-free technique that is able to discriminate between 6-OAU and DL-175 (Lucy et al., 2019). In this assay, the seeding of cells into wells containing a microarray of electrodes introduces an electrical resistance (measured as cell index), which increases upon cell attachment and proliferation (Fig. 2A and B) (Atienza et al., 2005). In mBMDMs and human U937 cells the impedance response to 1 μM DL-175 is more sustained than that for 6-OAU (Lucy et al., 2019).

In order to determine if the distinct impedance traces of 6-OAU and DL-175 in primary cells could be recapitulated in CHO cells we tested
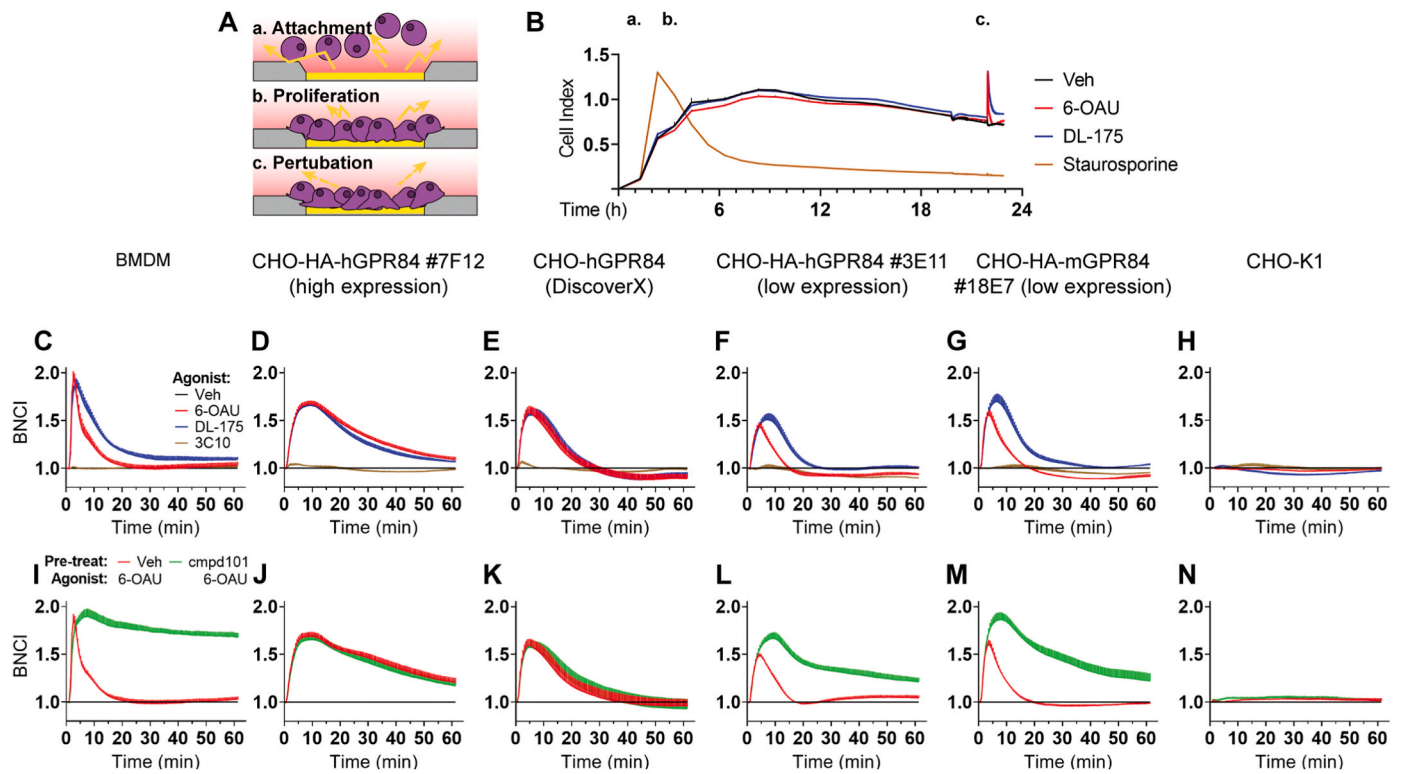
Fig. 2. GPR84 agonists 6-OAU and DL-175 elicit distinct impedance phenotypes in BMDMs and heterologous CHO expression systems. (A) Cells are seeded into 96-well xCELLigence E-plates containing a microarray of gold electrodes. (B) Cell index measurements are taken on cells incubated overnight as they attach and proliferate. Staurosporine (600 nM) was added 1 h after cell seeding to demonstrate the effect of cytotoxic pressure. Cells were plated 22 h prior to stimulation with 1 μM 6-OAU or DL-175 (C–H), or pre-treated for 2 h with 30 μM cmpd101 or vehicle followed by stimulation with 1 μM 6-OAU (I–N). Cell index values were normalised to baseline conditions (Veh, C–H; Veh-Veh, I–N). Lines depict mean ± SEM, n = 3, each experiment performed in duplicate. BMDM, bone marrow-derived macrophage; BNCI, baseline normalised cell index; 3C10, 3-hydroxy capric acid.

the newly developed CHO-GPR84 cell lines in CEI assays. The mBMDM response to DL-175 was characterised by a delayed decay in signal compared to 6-OAU (Fig. 2C) which could be recapitulated in both human and mouse cell lines with low receptor expression (Fig. 2F and G). Conversely, the high expressing and commercial hGPR84 cell lines exhibited a constitutively elevated signal in which 6-OAU and DL-175

had identical responses (Fig. 2D and E). The 6-OAU signal in the high expressing cell line remained elevated to 60 min, in the commercial cell line it had reached baseline by 30 min, and in the low expressing cell lines it had decayed by 15 min, paralleling the decay of the mBMDM response at 20 min. Furthermore, pre-incubation with the GRK2/3 inhibitor compound 101 augmented the positive impedance response
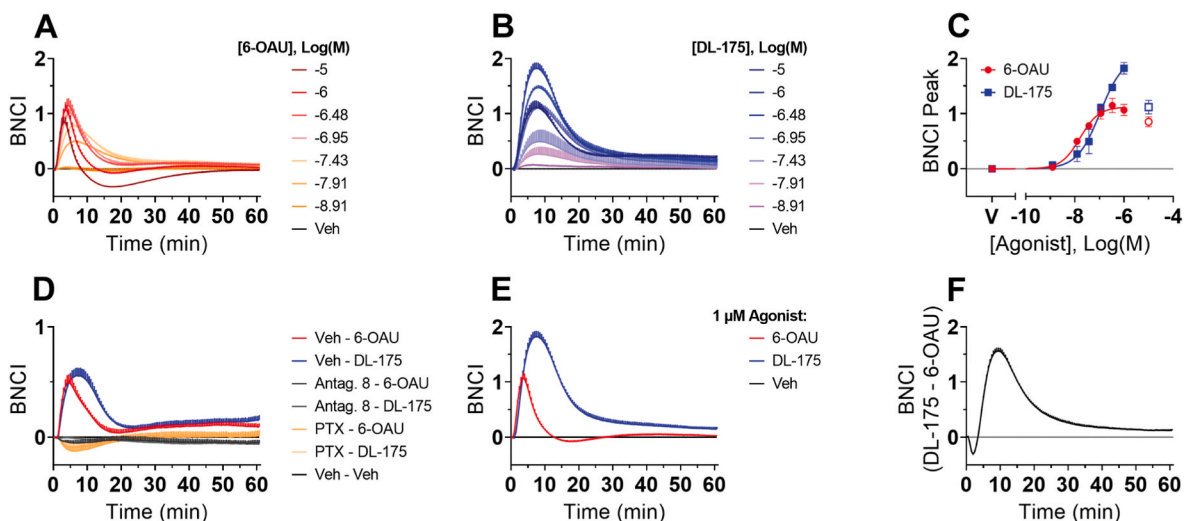
Fig. 3. Similarities and differences between 6-OAU and DL-175 in the GPR84 impedance response. CHO-HA-hGPR84 #3E11 low expressing cells were seeded 20–22h prior to stimulation with varying concentrations of 6-OAU (A) or DL-175 (B). (C) Peak BNCI values from A and B plotted as concentration-response curves. (D) Responses to 1 μM 6-OAU or DL-175 following 2 h pre-incubations with antagonist 8, pertussis toxin, or vehicle. (E) Comparison of the 1 μM responses from A and B. (F) Differences between the 1 μM impedance responses in E, achieved by subtracting the 6-OAU response from the DL-175 response. Lines depict mean ± SEM, n = 3, each experiment performed in duplicate. BNCI, baseline normalised cell index.

elicited by 6-OAU in mBMDMs (Fig. 2I) and low expressing cell lines (Fig. 2L and M), but not the high expressing or commercial cell lines (Fig. 2J and K). Responses to 6-OAU and DL-175 are absent in GPR84 KO mBMDMs (Lucy et al., 2019) and lacked any signal in CHO–K1 parental cells (Fig. 2H, N).

3.3. The impedance responses linked to 6-OAU and DL-175 show differential kinetics

Impedance sensing is a kinetic and label-free technique that is able to discriminate between 6-OAU and DL-175 in primary cells and low expressing cell lines. Results using agonists at 1 μM indicate that the responses in mBMDMs and human U937 cells (Lucy et al., 2019) were translatable to CHO cells and do not differ between human and mouse orthologues (Fig. 2). Therefore, we sought to characterise these ligands more thoroughly using kinetic assays in the CHO-HA-hGPR84 #3E11 low expressing cell line.

Treatment with 6-OAU and DL-175 caused concentration-dependent increases in the maximum signal of the initial BNCI peak (Fig. 3A and B). Notably, the distinct phenotypes were consistent across concentrations, and it was evident that titrating agonists to an equivalent signal peak would not result in similar curve shapes. Concentration-response curves generated using BNCI peak maxima showed both ligands elicited similar low nanomolar EC_{50}'s (Fig. 3C). The response of 6-OAU, $EC_{50} = 15.2$ nM ($pEC_{50} = 7.82 \pm 0.13$), and DL-175, $EC_{50} = 83.5$ nM ($pEC_{50} = 7.08 \pm 0.20$) were similar to their cAMP potencies in the same cell line (15.4 nM and 29.0 nM) and potencies previously determined in mBMDMs (129 nM and 50.3 nM) (Lucy et al., 2019). The peak signal elicited by DL-175, $E_{max} = 1.82$, was found to be 1.6-fold higher than 6-OAU, $E_{max} = 1.15$. The specificity of each response was demonstrated by pre-treatment and blockade of effect using antagonist 8 and pertussis toxin (Fig. 3D).

Comparison of the responses elicited by 1 μM agonist highlights the differences between DL-175 and 6-OAU in terms of the max signal and the sustained response of DL-175 (Fig. 3E). We further analysed these traces and found that the slopes of the ascending and descending phases were almost identical (Table 2). Both ligands caused rapid increases in the first 3 min. DL-175 then exhibits a delay in the impedance peak time (7.5 min), which occurs 4 min after the peak of 6-OAU (3.5 min). This delay is concomitant with delays in the ascending and descending slopes, as well as a greater area under curve (Table 2). In addition to differences at 1 μM, these delays were also present at all other concentrations tested between 10 nM and 10 μM. To highlight these kinetic differences in impedance responses we subtracted the 6-OAU response from the DL-175 response (Fig. 3F). It is evident that the agonists exhibit similar responses within 3.5 min of addition, before rapidly diverging such that they are most different near the 10 min time point. The signals then converge and continue to signal at comparable levels from approximately 30 min onwards (Fig. 3F). Just as high expression systems might mask subtle differences between agonists, long time points

Table 2
Comparison of the GPR84 impedance responses to 1 μM 6-OAU and DL-175.

Descriptor	6-OAU	DL-175	Significance
AUC (min × BNCI)	6.8 ± 0.6	32 ± 1	****
Peak time (min)	3.528 ± 0.006	7.5 ± 0.3	***
Max slope, Ascending (BNCI / min)	0.56 ± 0.05	0.55 ± 0.05	ns
time of max slope ascending (min)	1.747 ± 0.006	2.4 ± 0.2	*
Max slope, Descending (BNCI / min)	−0.24 ± 0.02	−0.17 ± 0.04	ns
Time of max slope descending (min)	5.29 ± 0.01	12.7 ± 0.3	****

Unpaired t-test P-values: ≤0.0001 (****), ≤0.001 (***), ≤0.01 (**), ≤0.05 (*), >0.05, ns. All units given as mean ± SEM, n = 3. AUC, area under curve; BNCI, baseline normalised cell index.

might miss key times in which the DL-175 and 6-OAU G-protein-mediated responses differ, highlighting the importance of kinetic readouts in assays for signalling bias.

3.4. Similarities and differences in ERK and Akt activation following treatment with 6-OAU and DL-175

Due to the time-dependent distinction between 6-OAU and DL-175 in impedance assays we sought to characterise the ability of these two agonists to activate ERK and Akt, two transiently activated downstream kinases canonically linked to GPCRs as well as to GPR84 specifically (Peters et al., 2022; Recio et al., 2018). We compared ERK and Akt phosphorylation in the high expressing and low expressing cell lines by separating proteins by SDS-PAGE and simultaneously probing for total- and phospho-protein. The same cell lysates were used to probe for ERK and Akt. Following agonist incubations for various time points we found that both 6-OAU and DL-175 caused transient responses that were absent in CHO–K1 parental cells (data not shown).

In the high expressing human GPR84 #7F12 cell line both agonists caused similar peaks in Akt phosphorylation at 10 min (Fig. 4A, C). In contrast, the low expressing #3E11 cell line responded to 6-OAU with a peak in Akt activation at 5 min, compared to the delayed and suppressed peak of DL-175 occurring at 10 min (Fig. 4B, D). Stimulation with 6-OAU also caused greater Akt activation at 5 min in the low expressing mouse GPR84 #18E7 cell line (Figs. S5C and D). In the case of GPR84-mediated ERK activation both 6-OAU and DL-175 caused similar responses with peaks at or near 5 min in both the high and low expressing human GPR84 cell lines (Fig. 4E–H). Furthermore, the ERK and Akt responses were notably prolonged in the high expressing human GPR84 cell line when compared to the low expressing cell line (Fig. 4).

3.5. 6-OAU promotes greater GPR84 internalisation than DL-175

Having established that the GPR84 agonist DL-175 exhibits signalling bias through multiple pathways, we sought to explore whether this could be correlated with differences in the subcellular localisation of the receptor that could lead to changes in signalling. Assays for surface receptor expression were conducted by quantifying reductions in surface-accessible HA-tag on high expressing HA-hGPR84 cells.

Both 6-OAU and DL-175 caused reductions in plasma membrane receptor over time in a concentration-dependent manner (Fig. 5A–C). The reduction was more pronounced upon treatment with 6-OAU than DL-175. Expectedly, these effects were lost upon blocking internalisation with agonist treatment at 4 °C (data not shown). At 1 μM 6-OAU achieved a significantly lower plateau than DL-175, but did not achieve this lower plateau faster than DL-175 (Fig. 5D, Table 3). The slight differences in one-phase decay half-lives and rate constants indicate that treatment with 1 μM 6-OAU reaches a steady state of 70% surface receptor in approximately 30 min (4 half-lives), compared to DL-175 which takes a longer time (>50 min) to reach the level of 89% surface receptor compared to vehicle. The marked differences between agonists were plotted by subtracting 6-OAU from DL-175, which underscores the way in which 6-OAU rapidly ($t_{1/2} = 5$ min) achieved and sustained greater reductions in nett surface receptor than DL-175 (Fig. 5E).

DL-175 fails to cause equivalent reductions in nett surface receptor as 6-OAU, even when incubated for long periods at higher concentrations. The concentration response-curves at 1 h, modelled using 3-parameter fitting, highlight the greater efficacy and potency of 6-OAU (Fig. S6J, Table 3). Reductions in surface receptor were not observed with other GPR84 agonists capric acid and 3-hydroxy capric acid (Figs. S6F, G, K). No reductions were seen with antagonist 8 (GPR84 antagonist), myristic acid (non-efficacious MCFA), and DL-222 (inactive analogue of DL-175) when compared to either vehicle (DMSO) or no vehicle (buffer only) (Fig. S6K). Finally, pre-treatment with antagonist 8 was able to abrogate these reductions in nett surface receptor (Fig. S6L).
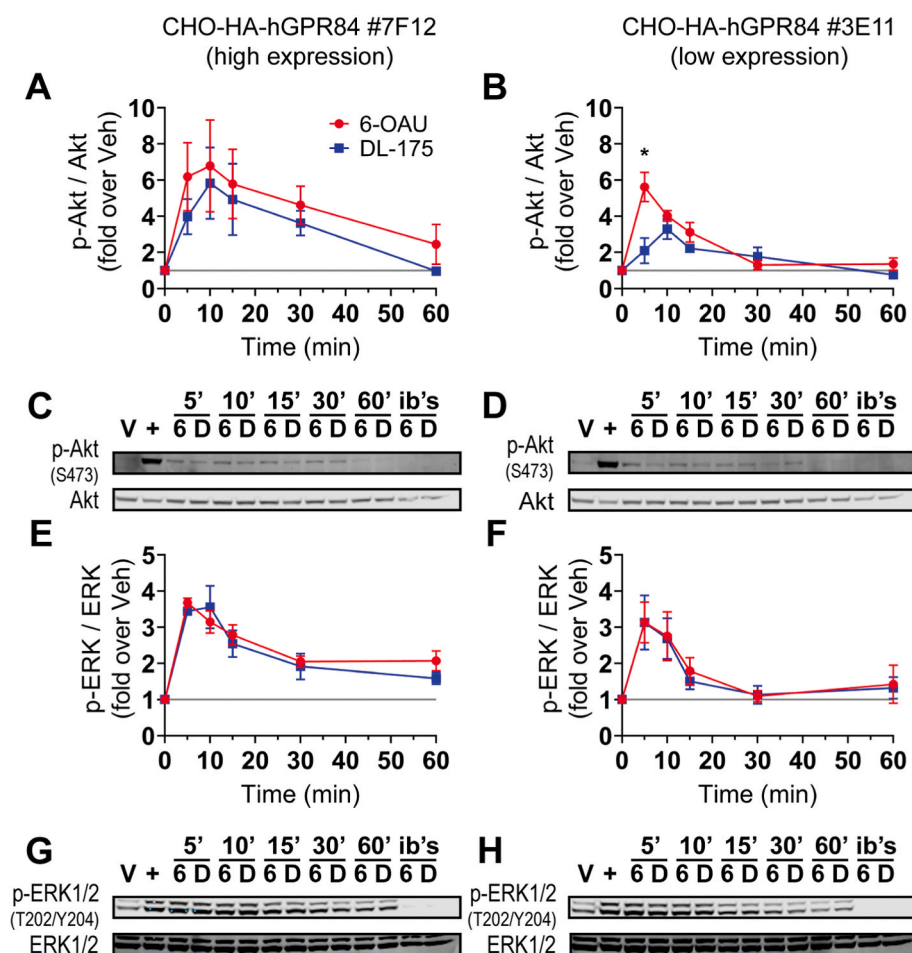
Fig. 4. Time course of GPR84-mediated ERK and Akt activation. CHO-HA-hGPR84 #7F12 high expressing cells (A, C, E, G) or CHO-HA-hGPR84 #3E11 low expressing cells (B, D, F, H) were stimulated with 6-OAU or DL-175 (1 μM) for 5–60 min before cell lysis and protein detection by Western blot. Phosphorylated ERK or Akt was normalised to total ERK or Akt respectively, then expressed as fold-change over the vehicle condition at 10 min. Points represent mean ± SEM, n = 3. Unpaired T-test between 6-OAU and DL-175, P ≤ 0.05 (*). Representative Western blots shown underneath in black and white by separating the 700 nm and 800 nm near-infrared channels for clarity. V, vehicle; +, positive control (Calyculin A and FBS); ib's, inhibitors (MK-2206 and U0126); 6, 6-OAU; D, DL-175.

4. Discussion

GPR84 couples to $G_{i/o}$ G-proteins and the MCFA capric acid has been shown to be active at both human and mouse GPR84, which share 85% amino acid identity (Marsango et al., 2022a; Wang et al., 2006). We have shown under standardised assay conditions that both 6-OAU and DL-175 elicit specific low nanomolar cAMP responses at both human and mouse GPR84. The apparent stimulation of cAMP production at high concentrations of 6-OAU may represent off-target activity or a switch in G-protein coupling. However, this was not observed in the high expressing cell lines where G-protein promiscuity might be expected to be more pronounced (Finlay et al., 2017). These cAMP data are only indicative of nett cAMP production at the 30 min time point, and further experiments, especially those employing kinetic readouts, would be needed to determine the conditions under which GPR84 begins to couple to other G-proteins. Furthermore, this cAMP assay has a ceiling on the maximal inhibition of forskolin-stimulated cAMP production that a compound can induce, which may be masking efficacy differences between 6-OAU and DL-175. In the case of the putative agonists capric acid and 3-hydroxy capric acid, our results suggest that only in systems of high receptor expression will they cause full efficacy cAMP responses. Whether these high levels of expression are achieved *in vivo* remains to be demonstrated. Nonetheless, evaluating ligands in systems with varying expression levels of their cognate receptor is important for a more complete pharmacological characterisation (Kenakin, 2007; Moran et al., 2018).

Label-free techniques are known to be able to detect the activation of GPCRs at endogenous expression levels. Leung et al. (2005) observed that the impedance signal from CHO cells overexpressing dopamine and muscarinic GPCRs were not higher than those from endogenously expressed serotonin, calcitonin, or prostaglandin receptors. We provide an extension of this observation in showing that the signal magnitude is not different between high and low expression levels of the same receptor, GPR84. When considering the phenotype of the CEI signals over time, however, there were clear differences between CHO cell lines bearing different GPR84 expression levels. Notably, the high expressing cell line exhibits a sustained signal, suggesting there is substantial receptor reserve involved and that cells treated with 6-OAU, DL-175, and 6-OAU with cmpd101 reach and maintain a maximum system efficacy. The maintenance of this signal elevation corresponds to the rank ordered cAMP potency: CHO-HA-hGPR84 #7F12 (high expression) > CHO-hGPR84 (DiscoverX) > CHO-HA-hGPR84 #3E11 (low expression), which supports the observation that G-protein-dependent effects are the primary influencers of the CEI response (Doijen et al., 2017). We therefore predict that lowering receptor expression releases the sustained signalling imparted by a system with high receptor reserve and allows for the measurement of higher fidelity cell impedance responses. Our observation that the low expressing cell lines phenocopy mBMDMs is consistent with a low receptor reserve and more physiological receptor-effector coupling. One consequence of this prediction would be that the overexpression of effector proteins, such as promiscuous G-proteins or fusion constructs, would negatively impact the fidelity of label-free responses.

Our data show that the 6-OAU and DL-175 impedance responses have significant differences in peak and decay time but not in curve shape or direction. In contrast, β-adrenergic receptor ligands can be discretely classified by impedance phenotype at the $β_2$-adrenergic receptor (Stallaert et al., 2012), as can synthetic and endogenous
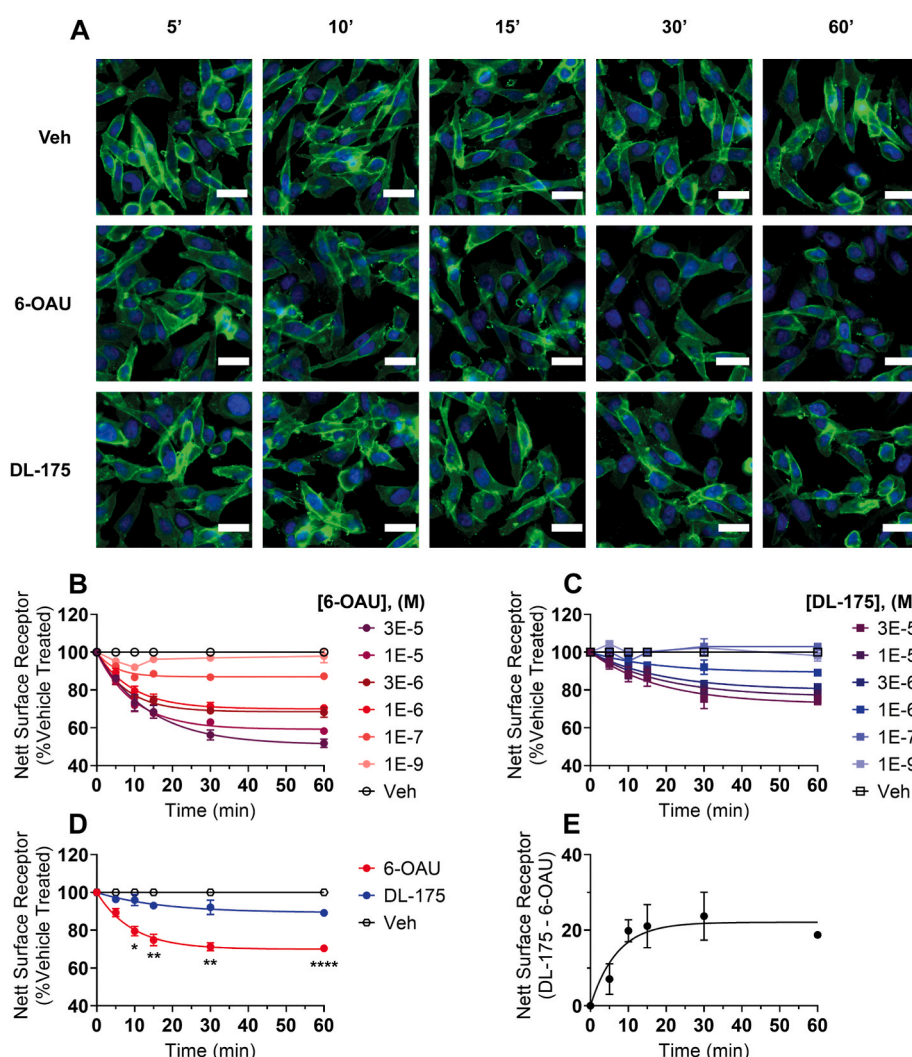
Fig. 5. Agonist-induced reductions in the nett surface expression of GPR84. (A) CHO-HA-hGPR84 #7F12 high expressing cells were stimulated with 6-OAU or DL-175 (1 μM) for 5–60 min before fixation without membrane permeabilisation and stained for the HA-tag (green) and nuclei (blue). Images acquired using a 20X 0.75 NA objective lens, scale bar = 25 μm. Quantification of the green channel fluorescence intensity in segmented cell masks show reductions in nett surface receptor following treatment with varying concentrations of 6-OAU (B) or DL-175 (C). (D) Comparison of the reductions in nett surface receptor using 1 μM agonist from B and C. (E) Differences between the 1 μM responses in D, achieved by subtracting the 6-OAU response from the DL-175 response. Points represent mean ± SEM, n = 3, each experiment performed in triplicate. Unpaired T-test between 6-OAU and DL-175 P-values: ≤ 0.0001 (****), ≤ 0.001 (***), ≤ 0.01 (**), ≤ 0.05 (*), >0.05, ns.

Table 3

Comparison of the agonist-induced reductions in surface GPR84 following treatment with 6-OAU or DL-175.

Data Set	Descriptor	6-OAU	DL-175	Significance
1 μM agonist (Fig. 5D)	Plateau (Nett Surface Receptor, %Veh treated)	70 ± 1	89 ± 1	***
1 μM agonist (Fig. 5D)	K (min⁻¹)	0.11 ± 0.02	0.06 ± 0.02	ns
1 μM agonist (Fig. 5D)	$t_{1/2}$ (min)	7 ± 1	13 ± 4	ns
CRC (Fig. S6J)	E_{max} (%Internalised)	45 ± 1	27 ± 2	**
CRC (Fig. S6J)	pEC_{50}	6.1 ± 0.1	5.73 ± 0.08	*

Unpaired *t*-test P-values: ≤ 0.0001 (****), ≤ 0.001 (***), ≤ 0.01 (**), ≤ 0.05 (*), >0.05, ns. All units given as mean ± SEM, n = 3. CRC, concentration-response curve.

cannabinoids acting at the CB_2 receptor (Hillger et al., 2017). Furthermore, a snapshot of the huge repertoire of GPCR-mediated impedance responses can be seen in the extensive review by Doijen et al. (2019). In light of the large diversity of possible impedance responses, our data suggests that 6-OAU and DL-175 engage similar downstream targets, but do so with different kinetics. A similar observation was made by Peters et al. (2022) who have shown, using an analogous optical label-free technology, that capric acid elicits a more sustained response than 3-hydroxy capric acid at GPR84. Experiments to determine the impedance

responses of a broader range of ligands may further furnish the GPR84 space with impedance phenotypes of interest.

It is an emerging consensus that G_i-coupled GPCRs cause positive impedance signals (Doijen et al., 2019). GPCR-β-arrestin signalling, on the other hand, appears to be more likely to alter the kinetics of the impedance response or cause more subtle changes in the trace without altering the primary peak responses (Doijen et al., 2017; Kammermann et al., 2011; Watts et al., 2012). Our results are consistent with these findings, as the distinct phenotype of DL-175 was governed largely by kinetics, and the EC_{50}'s derived from impedance maxima correlated well with cAMP EC_{50}'s. Furthermore, this phenotype was apparent at concentrations ranging from 10 nM up to 10 μM. Notably, at or below 1 μM neither agonist is able to recruit β-arrestin in the recombinant assay (Fig. S7). Yet, we have observed phenotypic impedance differences at 1 μM as well as at low nanomolar concentrations. We hypothesise that this could be due to differences in recruitment of the GRK2/3 kinases, which are negative regulators of G_i-pathway signalling and known to phosphorylate GPR84 (Marsango et al., 2022b). The phosphorylation of GPR84 and inhibition of G_i-pathway signalling could be responsible for the kinetic differences in the impedance trace without necessarily leading to the recruitment of β-arrestin which only occurs at higher concentrations.

Downstream ERK and Akt phosphorylation time courses have revealed the presence of a temporal signalling bias of DL-175, which promotes ERK activation but has a diminished ability to activate Akt. This outcome is dependent on both time and receptor expression, and

therefore was only seen in our low expressing cell line and only at the 5 min time point. Additionally, this bias was evident with agonists at 1 μM, below the concentration of detectable β-arrestin signalling with these agonists (Lucy et al., 2019) (Fig. S7). It has recently been shown that GPR84 signalling via G_{a15} results in ERK activation and ROS production in macrophages while Akt is driven by $G_{\alpha i}$ (Peters et al., 2022). This delineation of ERK versus Akt signalling provides a conceivable rationale that this bias exists at the level of G-protein coupling. While our studies have utilised a low expressing CHO-HA-hGPR84 cell line, we expect this effect to translate to other primary cells. At the same concentration of 1 μM, 6-OAU has been shown to activate Akt in mBMDMs in a time course that mirrors our low expressing cell line; a peak at 5–10 min which has decayed by 30 min (Recio et al., 2018). ERK phosphorylation in mBMDMs has a similar peak at 10 min, but appears to display a second peak at 60 min which we did not see in CHO cells (Recio et al., 2018). Other agonists have been used to show that GPR84 agonists activate ERK and Akt in human macrophages and THP-1-M1 macrophages (Gaidarov et al., 2018; Peters et al., 2022).

The pathways resulting in receptor internalisation dictate changes in surface expression over time, which result in an altered cell responsiveness to extracellular ligands. Due to the major influence assay time points have on signalling bias (Klein Herenbrink et al., 2016; Oyagawa et al., 2018), and given the known challenges when comparing agonist-induced internalisation at any single time point (Zhu et al., 2019), we tested for receptor internalisation at multiple time points and agonist concentrations within 60 min. To date, observations of GPR84 internalisation following treatment with 6-OAU, ZQ-16, embelin, and 2-HTP have been primarily qualitative (Gaidarov et al., 2018; Marsango et al., 2022b; Suzuki et al., 2013; Zhang et al., 2016). We have demonstrated through quantifying reductions in surface GPR84 that treatment with 6-OAU promotes greater GPR84 internalisation than DL-175. Treatment with 1 μM agonist shows that 6-OAU internalisation rapidly diverges from DL-175 within 10 min. Furthermore, the MCFAs capric acid and 3-hydroxy capric acid were tested at 100x their cAMP EC_{50}'s and did not result in significant internalisation. This is in line with reports that surface receptor expression was increased in CHO cells and unchanged in HEK cells following treatment with 100 μM capric acid and 3-hydroxy capric acid (Peters et al., 2020).

GPCR internalisation is canonically linked to the phosphorylation of the C-terminal tail and/or intracellular loops and the subsequent recruitment of β-arrestin. These changes to the intracellular core of the receptor act in concert to both arrest G-protein signalling and initiate new molecular pathways (Choi et al., 2018). In line with this sequence of events, it has been shown that activation with DL-175 fails to phosphorylate two key threonine resides in the third intracellular loop of GPR84 that are required for agonist-induced internalisation (Marsango et al., 2022b). Furthermore, we and others have reported the low potency of 6-OAU and lack of efficacy of DL-175 in β-arrestin recruitment assays (Fredriksson et al., 2022; Marsango et al., 2022b; Mårtensson et al., 2021). By quantifying cell surface receptor over time, we show that GPR84 undergoes robust agonist-induced internalisation at concentrations of agonist (e.g. 1 μM 6-OAU) that do not show detectable β-arrestin recruitment (Fig. S7), suggesting that GPR84 might be internalised in a β-arrestin-independent manner. This was also suggested by a previous observation that inhibition of the β-arrestin/AP-2 endocytic complex has no effect on the surface expression of GPR84 in CHO cells (Peters et al., 2020). Other G_i-coupled immune cell GPCRs are known to internalise in a β-arrestin-independent manner, such as FPR2 (Sundqvist et al., 2020). However, many questions remain unanswered regarding the mechanism of GPR84 internalisation and its effect on other signalling pathways.

5. Conclusions

An important hurdle towards unlocking the potential therapeutic value of GPR84 is a deeper understanding of which intracellular

signalling pathways it engages and the time course that it follows. DL-175 is known to lack GRK2/3-mediated phosphorylation of GPR84 (Marsango et al., 2022b), lack recruitment of the canonical GPCR desensitising protein β-arrestin (Lucy et al., 2019), and is now identified as having an impaired ability to internalise GPR84 as well as a suppressed downstream activation of Akt. These signalling differences were found to be transient, as DL-175 exhibited delays in both its impedance response and activation of Akt compared to 6-OAU. Importantly, these subtle differences in signalling kinetics could be masked by both long time points and high receptor expression, which cautions the use of long time points in stop time or accumulation assays. An altered subcellular localisation of GPR84 may give rise to an altered signalling repertoire, and our data highlight that this can be manipulated using biased agonists. Low micromolar concentrations of 6-OAU and DL-175 are sufficient to elicit differential signalling at early time points between 5 and 10 min in both transgenic and native expression systems such as mBMDMs. Therefore, the promotion or diminution of certain downstream pathways is achievable with specific biased agonists of GPR84, and the challenge remaining is to characterise the desirable and undesirable pathways in relevant cell types and contexts.

CRediT authorship contribution statement

Vincent B. Luscombe: Conceptualization, Methodology, Investigation, Writing – original draft. **Luis Alberto Baena-López:** Methodology, Writing – review & editing, Supervision. **Carole J.R. Bataille:** Investigation, Writing – review & editing. **Angela J. Russell:** Writing – review & editing, Project administration. **David R. Greaves:** Conceptualization, Writing – review & editing, Supervision, Project administration.

Declaration of competing interest

The authors declare no competing interests.

Data availability

Data will be made available on request.

Appendix A. Supplementary data

Supplementary data to this article can be found online at https://doi.org/10.1016/j.ejphar.2023.175960.

References

Atienza, J.M., Zhu, J., Wang, X., Xu, X., Abassi, Y., 2005. Dynamic monitoring of cell adhesion and spreading on microelectronic sensor arrays. SLAS Discovery 10, 795–805. https://doi.org/10.1177/1087057105279635.

Choi, M., Staus, D.P., Wingler, L.M., Ahn, S., Pani, B., Capel, W.D., Lefkowitz, R.J., 2018. G protein-coupled receptor kinases (GRKs) orchestrate biased agonism at the b2-adrenergic receptor. Sci. Signal. 11, eaar7084 https://doi.org/10.1126/scisignal.aar7084.

Cottin, V., Seemayer, C.A., Fagard, L., Ford, P., Van Der Aa, T., De Haas-Amatsaleh, A., Santermans, E., Sondag, E., Maher, T.M., Costabel, U., Strambu, I.R., 2021. Results of a phase 2 study of GLPG1205 for idiopathic pulmonary fibrosis (PINTA). Eur. Respir. J. 58, RCT2904. https://doi.org/10.1183/13993003.congress-2021.RCT2904.

Dahlgren, C., Gabl, M., Holdfeldt, A., Winther, M., Forsman, H., 2016. Basic characteristics of the neutrophil receptors that recognize formylated peptides, a

danger-associated molecular pattern generated by bacteria and mitochondria. Biochem. Pharmacol. 114, 22–39. https://doi.org/10.1016/j.bcp.2016.04.014.

Doijen, J., Van Loy, T., De Haes, W., Landuyt, B., Luyten, W., Schoofs, L., Schols, D., 2017. Signaling properties of the human chemokine receptors CXCR4 and CXCR7 by cellular electric impedance measurements. PLoS One 12, e0185354. https://doi.org/10.1371/journal.pone.0185354.

Doijen, J., Van Loy, T., Landuyt, B., Luyten, W., Schols, D., Schoofs, L., 2019. Advantages and shortcomings of cell-based electrical impedance measurements as a GPCR drug discovery tool. Biosens. Bioelectron. 137, 33–44. https://doi.org/10.1016/j.bios.2019.04.041.

Finlay, D.B., Cawston, E.E., Grimsey, N.L., Hunter, M.R., Korde, A., Vemuri, V.K., Makriyannis, A., Glass, M., 2017. Gαs signalling of the CB1 receptor and the influence of receptor number. Br. J. Pharmacol. 174, 2545–2562. https://doi.org/10.1111/bph.13866.

Finlay, D.B., Joseph, W.R., Grimsey, N.L., Glass, M., 2016. GPR18 undergoes a high degree of constitutive trafficking but is unresponsive to N-Arachidonoyl Glycine. PeerJ 4, e1835. https://doi.org/10.7717/peerj.1835.

Fredriksson, J., Holdfeldt, A., Mårtensson, J., Björkman, L., Møller, T.C., Müllers, E., Dahlgren, C., Sundqvist, M., Forsman, H., 2022. GRK2 selectively attenuates the neutrophil NADPH-oxidase response triggered by β-arrestin recruiting GPR84 agonists. Biochim. Biophys. Acta Mol. Cell Res. 1869, 119262 https://doi.org/10.1016/j.bbamcr.2022.119262.

Gaida, M.M., Dapunt, U., Hänsch, G.M., 2016. Sensing developing biofilms: the bitter receptor T2R38 on myeloid cells. Pathogens and Disease 74. https://doi.org/10.1093/femspd/ftw004.

Gaidarov, I., Anthony, T., Gatlin, J., Chen, X., Mills, D., Solomon, M., Han, S., Semple, G., Unett, D.J., 2018. Embelin and its derivatives unravel the signaling, proinflammatory and antiatherogenic properties of GPR84 receptor. Pharmacol. Res. 131, 185–198. https://doi.org/10.1016/j.phrs.2018.02.021.

Greaves, D.R., Schall, T.J., 2000. Chemokines and myeloid cell recruitment. Microb. Infect. 2, 331–336. https://doi.org/10.1016/S1286-4579(00)00293-8.

Hillger, J.M., le Roy, B., Wang, Z., Mulder-Krieger, T., Boomsma, D.I., Slagboom, P.E., Danen, E.H.J., Ijzerman, A.P., Heitman, L.H., 2017. Phenotypic screening of cannabinoid receptor 2 ligands shows different sensitivity to genotype. Biochem. Pharmacol. 130, 60–70. https://doi.org/10.1016/j.bcp.2017.01.014.

Kammermann, M., Denelavas, A., Imbach, A., Grether, U., Dehmlow, H., Apfel, C.M., Hertel, C., 2011. Impedance measurement: a new method to detect ligand-biased receptor signaling. Biochem. Biophys. Res. Commun. 412, 419–424. https://doi.org/10.1016/j.bbrc.2011.07.087.

Kenakin, T., 2007. Functional selectivity through protean and biased agonism: who steers the ship? Mol. Pharmacol. 72, 1393–1401. https://doi.org/10.1124/mol.107.040352.

Khalil, N., Manganas, H., Ryerson, C.J., Shapera, S., Cantin, A.M., Hernandez, P., Turcotte, E.E., Parker, J.M., Moran, John E., Albert, G.R., Sawtell, R., Hagerimana, A., Laurin, P., Gagnon, L., Cesari, F., Kolb, M., 2019. Phase 2 clinical trial of PBI-4050 in patients with idiopathic pulmonary fibrosis. Eur. Respir. J. 53, 1800663 https://doi.org/10.1183/13993003.00663-2018.

Klein Herenbrink, C., Sykes, D.A., Donthamsetti, P., Canals, M., Coudrat, T., Shonberg, J., Scammells, P.J., Capuano, B., Sexton, P.M., Charlton, S.J., Javitch, J.A., Christopoulos, A., Lane, J.R., 2016. The role of kinetic context in apparent biased agonism at GPCRs. Nat. Commun. 7, 10842 https://doi.org/10.1038/ncomms10842.

Labéguère, F., Dupont, S., Alvey, L., Soulas, F., Newsome, G., Tirera, A., Quenehen, V., Mai, T.T.T., Deprez, P., Blanqué, R., Oste, L., Le Tallec, S., De Vos, S., Hagers, A., Vandevelde, A., Nelles, L., Vandervoort, N., Conrath, K., Christophe, T., van der Aar, E., Wakselman, E., Merciris, D., Cottereaux, C., da Costa, C., Saniere, L., Clement-Lacroix, P., Jenkins, L., Milligan, G., Fletcher, S., Brys, R., Gosmini, R., 2020. Discovery of 9-cyclopropylethynyl-2-((S)-1-[1,4]dioxan-2-ylmethoxy)-6,7-dihydropyrimido[6,1-a]isoquinolin-4-one (GLPG1205), a unique GPR84 negative allosteric modulator undergoing evaluation in a phase II clinical trial. J. Med. Chem. 63, 13526–13545. https://doi.org/10.1021/acs.jmedchem.0c00272.

Leung, G., Tang, H.R., McGuinness, R., Verdonk, E., Michelotti, J.M., Liu, V.F., 2005. Cellular dielectric spectroscopy: a label-free technology for drug discovery. JALA: J. Assoc. Lab. Autom. 10, 258–269. https://doi.org/10.1016/j.jala.2005.06.002.

Lucy, D., Purvis, G.S.D., Zeboudj, L., Chatzopoulou, M., Recio, C., Bataille, C.J.R., Wynne, G.M., Greaves, D.R., Russell, A.J., 2019. A biased agonist at immunometabolic receptor GPR84 causes distinct functional effects in macrophages. ACS Chem. Biol. 14, 2055–2064. https://doi.org/10.1021/acschembio.9b00533.

Luscombe, V.B., Lucy, D., Bataille, C.J.R., Russell, A.J., Greaves, D.R., 2020. 20 Years an orphan: is GPR84 a plausible medium-chain fatty acid-sensing receptor? DNA Cell Biol. 39, 1926–1937. https://doi.org/10.1089/dna.2020.5846.

Marsango, S., Barki, N., Jenkins, L., Tobin, A.B., Milligan, G., 2022a. Therapeutic validation of an orphan G protein-coupled receptor: the case of GPR84. Br. J. Pharmacol. 179, 3529–3541. https://doi.org/10.1111/bph.15248.

Marsango, S., Ward, R.J., Jenkins, L., Butcher, A.J., Al Mahmud, Z., Dwomoh, L., Nagel, F., Schulz, S., Tikhonova, I.G., Tobin, A.B., Milligan, G., 2022b. Selective phosphorylation of threonine residues defines GPR84–arrestin interactions of biased ligands. J. Biol. Chem. 298 https://doi.org/10.1016/j.jbc.2022.101932.

Mårtensson, J., Sundqvist, M., Manandhar, A., Ieremias, L., Zhang, L., Ulven, T., Xie, X., Björkman, L., Forsman, H., 2021. The two formyl peptide receptors differently regulate GPR84-mediated neutrophil NADPH oxidase activity. J. Innate Immun. 13, 242–256. https://doi.org/10.1159/000514887.

McDonald, B., Pittman, K., Menezes, G.B., Hirota, S.A., Slaba, I., Waterhouse, C.C.M., Beck, P.L., Muruve, D.A., Kubes, P., 2010. Intravascular danger signals guide neutrophils to sites of sterile inflammation. Science 330, 362–366. https://doi.org/10.1126/science.1195491.

Moran, S.P., Cho, H.P., Maksymetz, J., Remke, D.H., Hanson, R.M., Niswender, C.M., Lindsley, C.W., Rook, J.M., Conn, P.J., 2018. PF-06827443 displays robust allosteric agonist and positive allosteric modulator activity in high receptor reserve and native systems. ACS Chem. Neurosci. 9, 2218–2224. https://doi.org/10.1021/acschemneuro.8b00106.

Moura-Alves, P., Puyskens, A., Stinn, A., Klemm, M., Guhlich-Bornhof, U., Dorhoi, A., Furkert, J., Kreuchwig, A., Protze, J., Lozza, L., Pei, G., Saikali, P., Perdomo, C., Mollenkopf, H.J., Hurwitz, R., Kirschhoefer, F., Brenner-Weiss, G., Weiner, J., Oschkinat, H., Kolbe, M., Krause, G., Kaufmann, S.H.E., 2019. Host monitoring of quorum sensing during *Pseudomonas aeruginosa* infection. Science 366, eaaw1629. https://doi.org/10.1126/science.aaw1629.

O'Leary, N.A., Wright, M.W., Brister, J.R., Ciufo, S., Haddad, D., McVeigh, R., Rajput, B., Robbertse, B., Smith-White, B., Ako-Adjei, D., Astashyn, A., Badretdin, A., Bao, Y., Blinkova, O., Brover, V., Chetvernin, V., Choi, J., Cox, E., Ermolaeva, O., Farrell, C. M., Goldfarb, T., Gupta, T., Haft, D., Hatcher, E., Hlavina, W., Joardar, V.S., Kodali, V.K., Li, W., Maglott, D., Masterson, P., McGarvey, K.M., Murphy, M.R., O'Neill, K., Pujar, S., Rangwala, S.H., Rausch, D., Riddick, L.D., Schoch, C., Shkeda, A., Storz, S.S., Sun, H., Thibaud-Nissen, F., Tolstoy, I., Tully, R.E., Vatsan, A. R., Wallin, C., Webb, D., Wu, W., Landrum, M.J., Kimchi, A., Tatusova, T., DiCuccio, M., Kitts, P., Murphy, T.D., Pruitt, K.D., 2016. Reference sequence (RefSeq) database at NCBI: current status, taxonomic expansion, and functional annotation. Nucleic Acids Res. 44, D733–D745. https://doi.org/10.1093/nar/gkv1189.

Oyagawa, C.R.M., de la Harpe, S.M., Saroz, Y., Glass, M., Vernall, A.J., Grimsey, N.L., 2018. Cannabinoid receptor 2 signalling bias elicited by 2,4,6-trisubstituted 1,3,5-triazines. Front. Pharmacol. 9, 1202. https://doi.org/10.3389/fphar.2018.01202.

Peters, A., Rabe, P., Krumbholz, P., Kalwa, H., Kraft, R., Schöneberg, T., Stäubert, C., 2020. Natural biased signaling of hydroxycarboxylic acid receptor 3 and G protein-coupled receptor 84. Cell Commun. Signal. 18, 31. https://doi.org/10.1186/s12964-020-0516-2.

Peters, A., Rabe, P., Liebing, A.-D., Krumbholz, P., Nordström, A., Jäger, E., Kraft, R., Stäubert, C., 2022. Hydroxycarboxylic acid receptor 3 and GPR84 – two metabolite-sensing G protein-coupled receptors with opposing functions in innate immune cells. Pharmacol. Res. 176, 106047 https://doi.org/10.1016/j.phrs.2021.106047.

Puengel, T., De Vos, S., Hundertmark, J., Kohlhepp, M., Guldiken, N., Pujuguet, P., Auberval, M., Marsais, F., Shoji, K.F., Saniere, L., Trautwein, C., Luedde, T., Strnad, P., Brys, R., Clément-Lacroix, P., Tacke, F., 2020. The medium-chain fatty acid receptor GPR84 mediates myeloid cell infiltration promoting steatohepatitis and fibrosis. J. Clin. Med. 9 https://doi.org/10.3390/jcm9041140.

Recio, C., Lucy, D., Purvis, G.S.D., Iveson, P., Zeboudj, L., Iqbal, A.J., Lin, D., O'Callaghan, C., Davison, L., Griesbach, E., Russell, A.J., Wynne, G.M., Dib, L., Monaco, C., Greaves, D.R., 2018. Activation of the immune-metabolic receptor GPR84 enhances inflammation and phagocytosis in macrophages. Front. Immunol. 9 https://doi.org/10.3389/fimmu.2018.01419.

Solly, K., Wang, X., Xu, X., Strulovici, B., Zheng, W., 2004. Application of real-time cell electronic sensing (RT-CES) technology to cell-based assays. Assay Drug Dev. Technol. 2, 363–372. https://doi.org/10.1089/adt.2004.2.363.

Stallaert, W., Dorn, J.F., van der Westhuizen, E., Audet, M., Bouvier, M., 2012. Impedance responses reveal β2-adrenergic receptor signaling pluridimensionality and allow classification of ligands with distinct signaling profiles. PLoS One 7, e29420. https://doi.org/10.1371/journal.pone.0029420.

Stringer, C., Wang, T., Michaelos, M., Pachitariu, M., 2021. Cellpose: a generalist algorithm for cellular segmentation. Nat. Methods 18, 100–106. https://doi.org/10.1038/s41592-020-01018-x.

Sundqvist, M., Christenson, K., Holdfeldt, A., Gabl, M., Mårtensson, J., Björkman, L., Dieckmann, R., Dahlgren, C., Forsman, H., 2018. Similarities and differences between the responses induced in human phagocytes through activation of the medium chain fatty acid receptor GPR84 and the short chain fatty acid receptor FFA2R. Biochim. Biophys. Acta Mol. Cell Res. 1865, 695–708. https://doi.org/10.1016/j.bbamcr.2018.02.008.

Sundqvist, M., Holdfeldt, A., Wright, S.C., Møller, T.C., Siaw, E., Jennbacken, K., Franzyk, H., Bouvier, M., Dahlgren, C., Forsman, H., 2020. Barbadin selectively modulates FPR2-mediated neutrophil functions independent of receptor endocytosis. Biochim. Biophys. Acta Mol. Cell Res. 1867, 118849 https://doi.org/10.1016/j.bbamcr.2020.118849.

Suzuki, M., Takaishi, S., Nagasaki, M., Onozawa, Y., Iino, I., Maeda, H., Komai, T., Oda, T., 2013. Medium-chain fatty acid-sensing receptor, GPR84, is a proinflammatory receptor. J. Biol. Chem. 288, 10684–10691. https://doi.org/10.1074/jbc.M112.420042.

von Chamier, L., Laine, R.F., Jukkala, J., Spahn, C., Krentzel, D., Nehme, E., Lerche, M., Hernández-Pérez, S., Mattila, P.K., Karinou, E., Holden, S., Solak, A.C., Krull, A., Buchholz, T.-O., Jones, M.L., Royer, L.A., Leterrier, C., Shechtman, Y., Jug, F., Heilemann, M., Jacquemet, G., Henriques, R., 2021. Democratising deep learning for microscopy with ZeroCostDL4Mic. Nat. Commun. 12, 2276. https://doi.org/10.1038/s41467-021-22518-0.

Waisman, A., Norris, A.M., Elías Costa, M., Kopinke, D., 2021. Automatic and unbiased segmentation and quantification of myofibers in skeletal muscle. Sci. Rep. 11, 11793 https://doi.org/10.1038/s41598-021-91191-6.

Wang, J., Wu, X., Simonavicius, N., Tian, H., Ling, L., 2006. Medium-chain fatty acids as ligands for orphan G protein-coupled receptor GPR84. J. Biol. Chem. 281, 34457–34464. https://doi.org/10.1074/jbc.M608019200.

Watts, A.O., Scholten, D.J., Heitman, L.H., Vischer, H.F., Leurs, R., 2012. Label-free impedance responses of endogenous and synthetic chemokine receptor CXCR3

agonists correlate with Gi-protein pathway activation. Biochem. Biophys. Res. Commun. 419, 412–418. https://doi.org/10.1016/j.bbrc.2012.02.036.

Zhang, Q., Yang, H., Li, J., Xie, X., 2016. Discovery and characterization of a novel small-molecule agonist for medium-chain free fatty acid receptor G protein–coupled receptor 84. J. Pharmacol. Exp. Therapeut. 357, 337–344. https://doi.org/10.1124/jpet.116.232033.

Zhu, X., Finlay, D.B., Glass, M., Duffull, S.B., 2019. Model-free and kinetic modelling approaches for characterising non-equilibrium pharmacological pathway activity: internalisation of cannabinoid CB1 receptors. Br. J. Pharmacol. 176, 2593–2607. https://doi.org/10.1111/bph.14684.